actuators

Article

Digital Hydraulic Transformer Concepts for Energy-Efficient Motion Control †

Helmut Kogler

Linz Center of Mechatronics GmbH, 4040 Linz, Austria; helmut.kogler@lcm.at; Tel.: +43-732-2468-6059

† Presented at the 12th Workshop on Digital Fluid Power 2024, Tampere, Finland, 6–7 June 2024.

Abstract: Hydraulic linear drive systems with conventional proportional valves result in poor energy efficiency due to resistance control. In systems with multiple actuators connected to one common pressure supply, a load-sensing strategy is often used to reduce these throttling losses. However, like conventional cylinder actuators, common load-sensing systems are also not able to recuperate the energy, which is actually released when a dead load is lowered. In order to overcome these drawbacks, in this paper, new concepts of a digital hydraulic smart actuator and a load-sensitive pressure supply unit are presented, which are qualified to reduce throttling losses and, furthermore, to harvest energy from the load. According to previous research, the basic concepts used in this contribution promise energy savings in the range of 30% for certain applications, which is one of the main motivations for this study. The operating principles are based on a parallel arrangement of multiple hydraulic switching converters, representing so-called digital hydraulic transformers. Furthermore, the storage module of the presented load-sensitive pressure supply unit is able to boost the hydraulic power in the common pressure rail beyond the maximum power of the primary motor. For exemplary operating cycles of the smart actuator and the pressure supply unit, a significant reduction in the energy consumption could be shown by simulation experiments, which offers a new perspective for energy-efficient motion control.

Keywords: digital fluid power; actuator; hydraulics; efficiency; recuperation; load sensing

Academic Editors: Matti Linjama and Tatiana Minav

Received: 20 December 2024
Revised: 20 January 2025
Accepted: 23 January 2025
Published: 25 January 2025

Citation: Kogler, H. Digital Hydraulic Transformer Concepts for Energy-Efficient Motion Control. *Actuators* **2025**, *14*, 54. https://doi.org/10.3390/act14020054

1. Introduction

Hydraulic drive technology has been well established for decades for heavy duty motion control, particularly in harsh environments, due to the robustness of the cylinder actuators. However, mobile applications, like, for instance, construction machines, suffer especially from bad energy efficiency if the common proportional valve control is applied. Of course, with load-sensing techniques, the throttling losses can be reduced, but if one supply unit is used for several actuators, then the minimum supply pressure is determined by the actuator with the highest load. This, in turn, leads to increased throttling losses at the actuators with lower loads. For this reason, more efficient actuator concepts are desirable. Furthermore, it is well known that the lowering of heavy loads, like, for instance, the boom of an excavator, presents a high potential for recuperable energy, which, unfortunately, cannot be reused with conventional hydraulic pressure supply units. One reason is that in common actuators, like conventional valve-controlled cylinders, the downstream fluid is always directed to tank and, thus, the potentially available energy is lost. In fact, so-called regenerative methods reduce the concomitant losses in the load-sensing system, but in today's valve-controlled machines, the potential energy of the dead load is mostly converted into heat during the lowering process by counterbalance valves or similar mechanisms. Since energy efficiency is becoming more and more important, the demand for recuperative supply systems is increasing (see, for instance, [1,2]). Of course, with conventional single-spool proportional valves, this cannot be achieved, but new control concepts with proportional independent metering, like those presented in [3–5] or [6], enable the opportunity to reuse the energy when heavy loads are lowered. With the independent metering approach, the in- and outflow of the cylinder chambers can be arbitrarily controlled, which offers the possibility to reuse fluid in a different pressure chamber and, thus, the overall energy consumption can be reduced. But only in very rare cases is it possible to direct fluid back to high-pressure supply lines for recuperation. A similar digital approach, realized with digital flow control units (DFCUs), can be found in [7]. In this context, a DFCU represents a parallel arrangement of numerous 2/2-directional switching valves with different sizes. The flow is controlled by certain combinations of valves with pulse code modulation. However, so far, with common independent metering approaches, only regenerative flow sharing between certain pressure chambers is possible, which, moreover, often requires a sophisticated control strategy.

A basic requirement for recuperation is the ability of the actuator, particularly, its actuation system, to direct the fluid back into the high-pressure supply line. In fact, this can be done also with simple independent metering, but only under certain load conditions with regard to the actual supply pressure. In most operating conditions, this specific functionality of boosting the pressure can only be reasonably realized with hydraulic transformers (see, for instance, [8–10]), which are able to boost pressure or flow in order to reduce throttling losses or recuperate energy. Basically, there exist two different types of hydraulic transformers: rotating transformers and valve-controlled transformers. The rotating transformers are based on variable pump/motor configurations, and the valve-controlled transformers often use a digital switching technique and certain inertance effects of specific components. A special class of digital hydraulic transformers (DHTs) is the so-called hydraulic buck converter (HBC), which represents an energy-efficient, pulse-width-modulated (PWM) switching concept transferred from power electronics to hydraulics and is mainly designed for cylinder actuators. Basically, this type of switching converter operates at a constant switching frequency of the order of 100 Hz and exploits the fluid inertia in a transmission line in order to efficiently step down or boost the pressure depending on the load conditions. Basic information concerning hydraulic switching converters can be found, for instance in [11–14]. An exemplary design study of such a prototypical realization is the HERCULES (acronym for Hydraulic Efficient and Robust Converter Unit for Linear motion under Energy Saving, which was introduced in [15]) actuator from [15] depicted in Figure 1a, which represents a so-called smart actuator, where the cylinder and valves for actuation are unified in one mechanical design. In contrast to former designs with prototypal components, the actuator from Figure 1a is solely realized with commercially available valves, which may bring the concept closer real applications.

In Figure 1b, the hydraulic scheme of the axis is illustrated with multiple converter stages arranged in parallel connected to the piston sided chamber of the cylinder. The converter stages are operated in a phase-shifted mode in order to reduce the pressure ripples caused by switching to an acceptable level, like in interleaved PWM actuated multi-phase DC-DC converters in power electronics (see, for instance, [16,17]). The rod sided chamber is either connected to supply pressure or tank pressure depending on the load conditions. In this specific application, shown in Figure 1, the high-speed switching valves are used for both moving directions. The directions of velocity (VD) and force (FD) are controlled by separate cheaper directional valves with lower dynamic requirements. In fact, with this configuration, an efficient motion control is possible; however, the switching of the force directional valves at the rod sided port of the cylinder results in unwanted spikes in the velocity due to the rapid compression or decompression of the rod sided pressure chamber. For this reason, in this paper, an improved concept of the smart actuator from Figure 1 is presented, which does not suffer from the mentioned deficiencies and is heceforth called HBC052 , as the second revision of the fifth generation of prototypes. With this kind of *smart* actuator, not only is an efficient drive operation resulting from reduced throttling losses due to flow boosting possible, but also, a recuperation of energy can be achieved due to pressure boosting over a wide operating range, which is not possible with today's valve-controlled systems. It is important to mention that, in turn, the supply system is required to be able to absorb fluid from the actuators. In the approach of a so-called common pressure rail (CPR) architecture, according to [18], this is possible, because the constant pressure supply is additionally equipped with accumulators, which are able to recover energy from different actuators, each controlled with a rotating hydraulic transformer like that presented in [19]. So far, on the excavator presented in [20], the mentioned transformers for metering the power are located in the body of the machine and not directly at the actuator. Consequently, each cylinder on the arm of the excavator must be connected via separate pipe lines with the transformer, which relativizes the basic idea of a common rail architecture, at least with regard to installation costs. In the already mentioned publication [15], an excavator arm equipped with efficient digital hydraulic actuators was investigated by simulation. As depicted in Figure 2a, the smart HERCULES actuators from Figure 1a are supplied by a real common rail system, which offers the possibility to share displaced oil volume between different consumers and, furthermore, to recuperate energy.

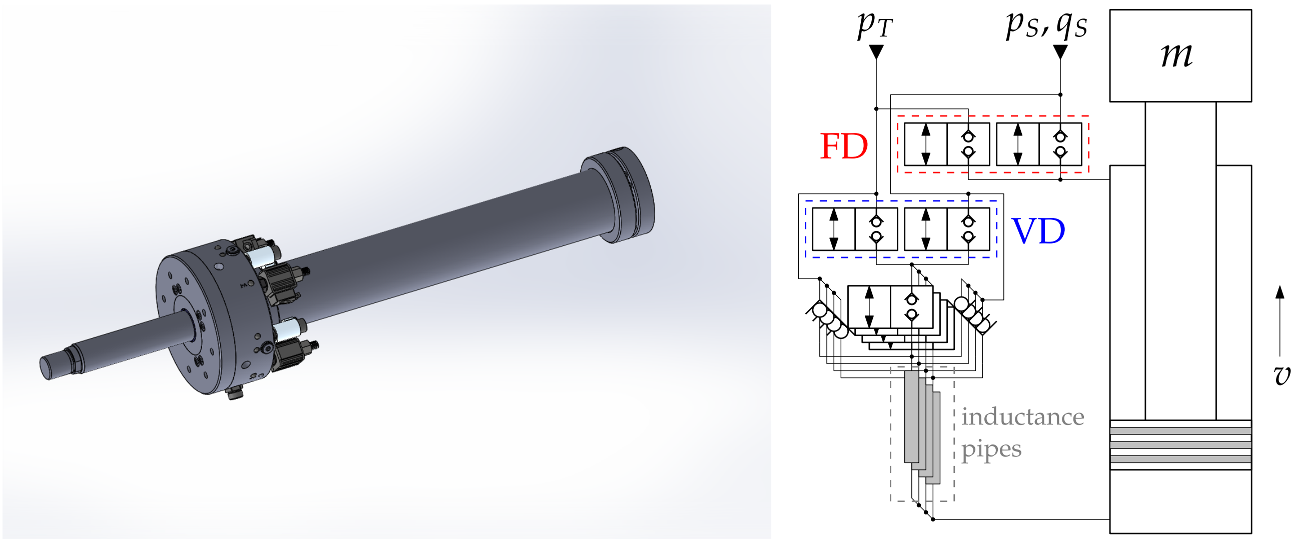

(**a**) (**b**)

Figure 1. HERCULES actuator from [15]. (**a**) Smart digital hydraulic actuator; (**b**) scheme with multiple buck converter stages.

In the mentioned study, compared to a conventional hydraulic proportional drive (HPD) with load sensing, a significant reduction in the energy consumption by 30% for a specific working cycle of a trench-digging operation (Figure 2b) could be shown with the smart actuator (HBC) by simulation. Compared to today's valve-controlled hydraulic drive systems, these results promise a highly economical and, moreover, an ecological operation of certain classes of construction machines, like excavators. It turns out that, for this kind of application, a load-sensitive pressure supply for controlling the pressure in the common rail system is beneficial for a reduction in the overall energy consumption.

However, a specific realization of such a pressure supply with the ability to store energy from the load was not discussed in the mentioned contribution. Therefore, in the following, a concept for a load-sensitive pressure supply with energy recuperation in combination with a load-sensitive common pressure rail (LS-CPR) is presented and discussed. The harvested energy is stored in a hydraulic gas-loaded accumulator using a DHT connected to the LS-CPR. Thus, energy can be recovered from any actuator in the system, which is not possible with other hydraulic buffer concepts, like that presented in [21], where the accumulator is only connected to the boom actuator. The proposed concept benefits not only from the promising reduced energy consumption, but also from a cost-effective design with fewer components, compared to hybrid excavators like that presented, for instance, in [22], where, additionally, electric components for energy conversion and storage must be spent. Furthermore, for an energy-efficient operation, a simple control strategy can be used. In the later-presented simulation experiments, the pressure p_S and the flow rate q_S of the power consumption regarding the trench-digging cycle depicted in the upper diagram of Figure 2b are used as input signals in order to demonstrate the tracking performance of the presented pressure supply concept. Both concepts, the HBC052 and the pressure supply unit with the buffer module, employ a DHT for efficiently stepping down the pressure or to boost the pressure over a significantly wider operating range than that provided by other concepts, like conventional independent metering. Furthermore, compared to rotational hydraulic transformers, a DHT can probably be realized at significantly lower costs.

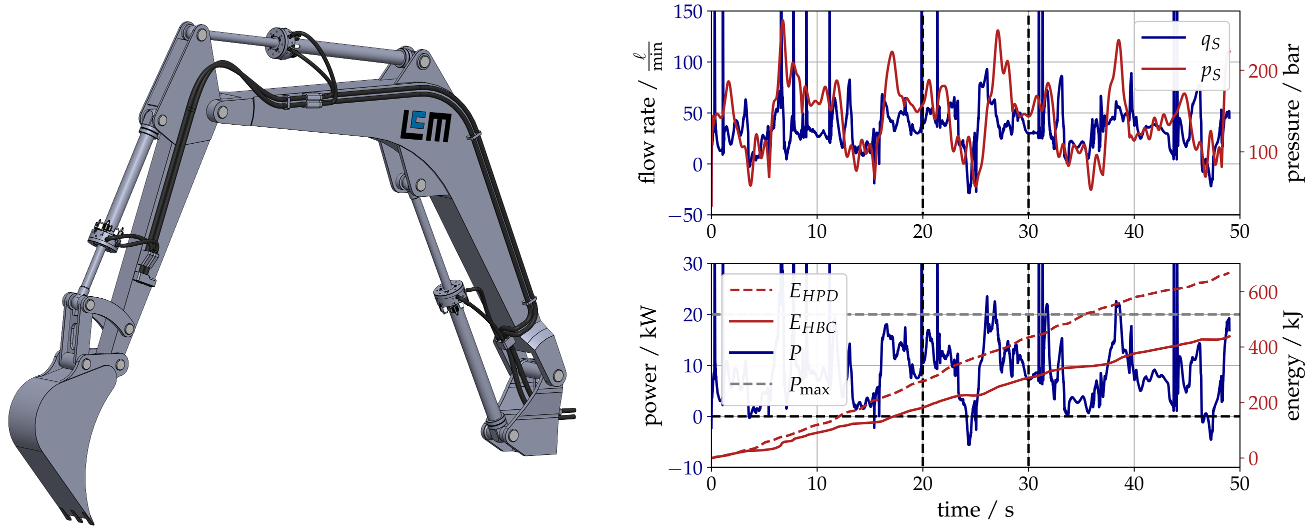

(**a**) (**b**)

Figure 2. Load-sensitive digital hydraulic application presented in [15]. (**a**) Excavator arm with common pressure rail architecture; (**b**) power consumption for the digging of a trench .

This article is a revised and expanded version of a paper [23], entitled "Efficient and Load-Sensitive Hydraulic Supply Unit using Multiple Switching Converters", which was presented at the Twelfth International Workshop on Digital Fluid Power [24] in Tampere, Finland in 2024. The original paper from [24] was devoted just to the basic concept of the digital hydraulic pressure supply unit for a simple exemplary load cycle. The mentioned contribution [23] was reworked and extended with significant content regarding the re-design and simulation of the digital hydraulic smart actuator and, furthermore, new simulation results for a realistic working cycle of the digital hydraulic supply unit were added.

2. Switching Concepts for Motion Control

In this section, the basic concepts investigated in this contribution are considered. At first, an improved conceptual re-design of the smart actuator from Figure 1b is introduced. Afterwards, the detailed concept of the pressure supply unit with a buffer module and a DHT is presented.

2.1. Re-Design of the Smart Actuator Concept

In Figure 3, a re-designed scheme of the digital hydraulic smart actuator (HBC052) for linear motion control is depicted. The major difference from the previous concept from Figure 1 is that, on the one hand, both pressure chambers are actuated by multiple switching converters, and on the other hand, the flow direction is controlled by separate switching valves, which halves the number of switching cycles of the fast switching valves and, thus, a significantly extended lifetime of the high-speed switching valves may be expected. The control value for one converter stage is a duty ratio, $0 \leq \kappa \leq 1$, which results in a pulse-width-modulated opening of the actuated switching valve; however, the flow through the converter must be controlled in both directions. Therefore, a flow from supply (p_S, p_T) to the load is realized by a positive duty ratio ($\kappa > 0$), which means that the high-pressure (p_S) sided switching valves are pulsed. In the negative flow direction ($\kappa < 0$), the tank sided valves are actuated, which results in a flow from the output of the converter to the supply (p_S, p_T). With regard to Figure 3, for an extending movement of the piston, the supply sided switching valves ($\kappa_1 > 0$) of cluster mHBC$_1$ and the tank sided valves ($\kappa_2 < 0$) of the other cluster, mHBC$_2$, are actuated simultaneously, but not necessarily with the same duty ratios κ_1 and κ_2, which represents an additional degree of freedom for control. Consequently, in the retracting direction, the opposite ($\kappa_1 < 0$, $\kappa_2 > 0$) is the case. Each transformer stage is operated in a phase-shifted pulse-width mode at a constant switching frequency, f_S. More details regarding the different operating modes of the transformers are presented later in Section 3.2.1, where the all operating modes of the digital hydraulic transformer for the buffer module are explained.

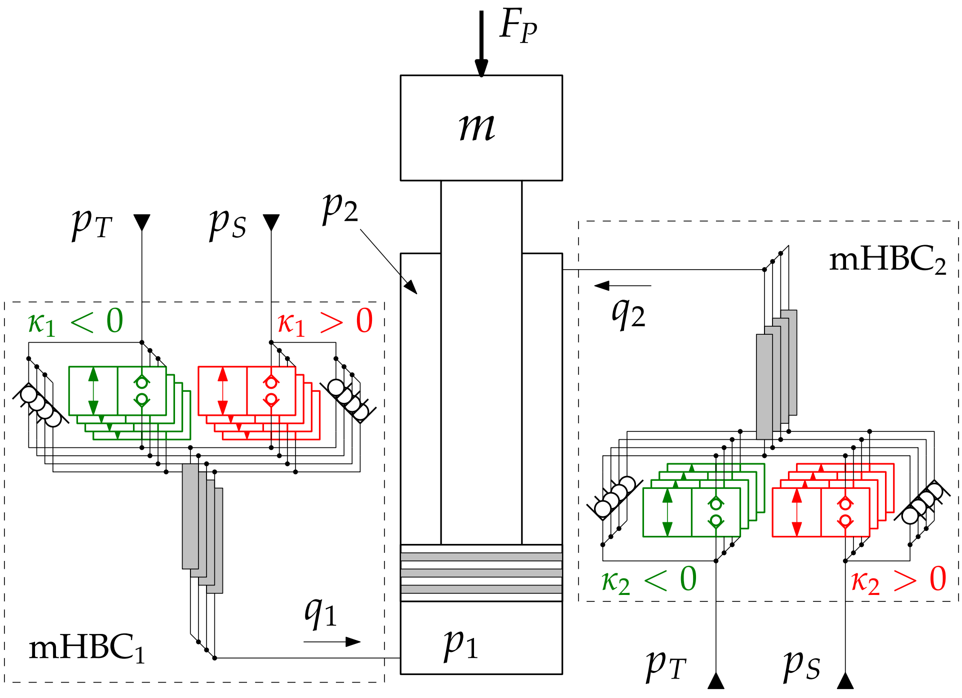

Figure 3. Digital hydraulic smart actuator (HBC052) with multiple hydraulic buck converters for each pressure chamber.

The separate transformer clusters for both chambers enable a decoupled control of velocity and force, which results in a smooth change of the power quadrants according to the load of the actuator during motion control. Figure 4 shows the control scheme, which is used in the simulations presented later on. The position is controlled by a simple proportional controller (P_x), with the transformer cluster connected to the piston sided chamber (mHBC$_1$) and, at the same time, the mean pressure p_1 in the piston sided chamber is controlled by a PI-controller (P_F, I_F) with the rod sided converter cluster mHBC$_2$. The basic strategy is that in the extending direction of movement, the pressure p_1 is controlled as close to tank pressure as possible, thus $p_1^d = p_T$. This results in a high-efficiency operation of transformer cluster mHBC$_1$, because in these operating conditions, the flow-boosting effect is very high, and much fluid can be drawn from the tank line. In the retracting moving direction, the pressure p_1 is controlled such that it is close to the supply pressure ($p_1^d = p_S$), because, in this case, the recuperation performance of cluster mHBC$_1$ is maximized. It is remarkable that for this simple control strategy, no knowledge of the actual load force F_P is required, which is presented later in the simulation section.

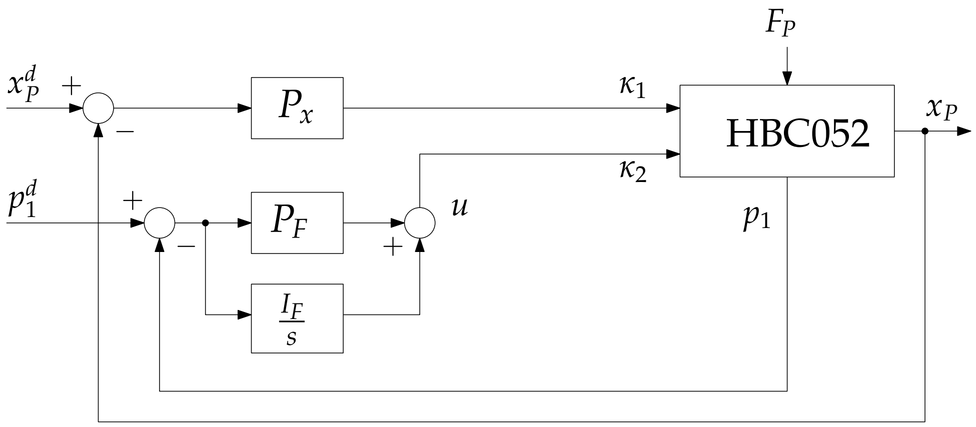

Figure 4. Control scheme of HBC052.

2.2. Load-Sensitive Pump Unit with a Buffer Unit for Energy Storage

In the following, the conventional standard load-sensing (LS) concepts of open, and, respectively, closed centers are completely dropped. It is assumed that all smart actuators supplied by the LS-CPR request a minimum desired supply pressure according to their actual states of operation. Thus, the pump being used is required to control its output pressure p_S, and the desired value of the supply pressure results in $p_S^d = \max(p_S^{\min 1}, \ldots, p_S^{\min \lambda})$, with λ as the number of actuators in the LS-CPR system. A convenient and efficient way to realize this goal is the application of a digital displacement pump (DDP, see, for instance, [25–27]). For simplicity and, furthermore, for cost reasons, it is assumed that the DDP is driven by a motor with constant speed and the pressure at the output p_S is controlled by the quantized flow ratio with regard to the maximum displacement volume according to the number of pistons of the DDP. This works perfectly in the delivering flow direction regarding controllability and efficiency. But since the motor and the used pump are not designed to change their direction of rotation, it is not possible to recuperate energy. Thus, a kind of a buffer module is necessary to store the recuperable energy, like that illustrated in Figure 5.

Of course, a sufficiently large gas-loaded accumulator must be used in the buffer module in order to store recuperable energy from the pressure rail. But, due to the actual working conditions of all actuators in the LS-CPR system, the supply pressure p_S varies faster than the buffer pressure p_B in the accumulator. Thus, a hydraulic transformer must be used. Furthermore, the desired supply pressure p_S can be either lower or higher than the pressure in the buffer accumulator. Thus, the hydraulic transformer must be able to operate in all four power quadrants.

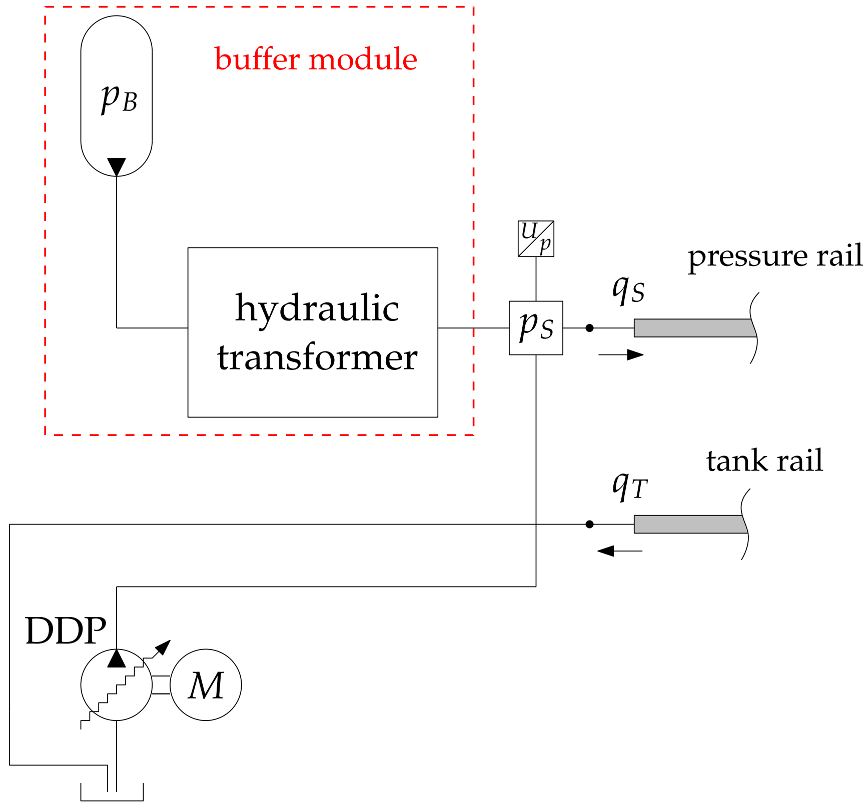

Figure 5. Load-sensitive pressure source using a digital displacement pump (DDP).

As explained in the previous paragraph, a hydraulic transformer must be installed between the buffer accumulator and the entry of the LS-CPR. One possibility is given by the well-known INNAS Hydraulic Transformer (IHT), according to [8], like that illustrated in Figure 6. Unlike other pump/motor transformers, the IHT is a single rotating machine with a constant displacement and a variable valve plate with three ports: a low-pressure port, a high-pressure port, and a port for the consumer pressure. Depending on the pressure levels at each port of the transformer and on the position of its valve plate, hydraulic energy can be either stored in the buffer accumulator or efficiently released to the LS-CPR by boosting the flow with fluid from the low-pressure accumulator. The tank pressure p_T is elevated in the range of approximately 10 bar with a pressure relief valve (PRV), and the low-pressure accumulator is charged with returning flow q_T from all the actuators in the system through the common tank rail. Moreover, if necessary, the transformer is able to boost the pressure in the LS-CPR up to double the pressure of the buffer accumulator.

The IHT seems to be a qualified device for transforming the power in the buffer module; however, there are some drawbacks, which must be critically reflected upon for some applications. The IHT operates according to an imposed pressure, which means that even a zero flow through the transformer must be actively controlled with the valve plate. Since the position of the valve plate is controlled by a separate electric servo motor, a limited response dynamics must be expected, at least to some extent. But, in contrast to the *soft* CPR, which provides an almost constant supply pressure, the LS-CPR represents a considerable *stiff* supply line, which may require a fast variation of the supply pressure in certain operating cases. Moreover, in case of a standstill, i.e., no delivery is intended, additional seat-type valves are necessary for load holding.

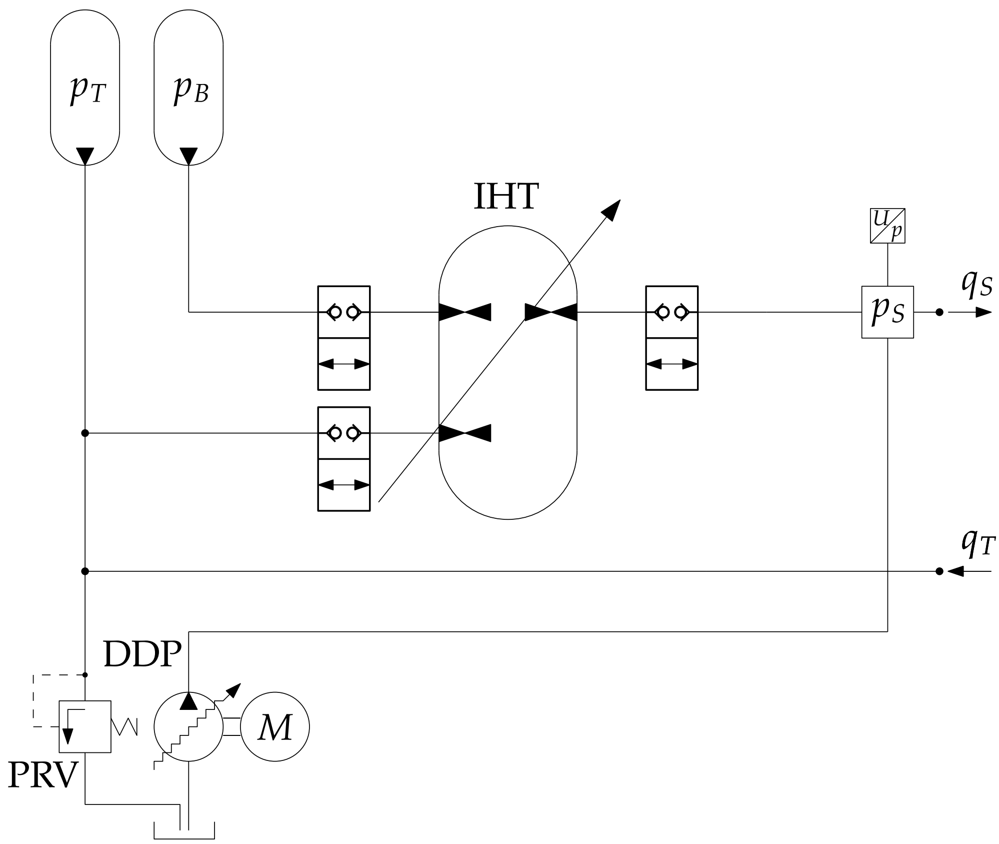

Figure 6. Load-sensitive supply unit with buffer module using an INNAS Hydraulic Transformer.

As an alternative, a digital hydraulic transformer (DHT) based on hydraulic switching converters, as shown in Figure 7, can be used, which is the focus of this contribution. The DHT represents a parallel arrangement of multiple buck–boost transformer stages, each consisting of four switching valves, four check valves, and one inductance pipe. In case of a standstill, i.e., no flow is desired at the consumers, all valves are shut and, therefore, no actuation is necessary, which fulfills the basic requirements for load holding. Depending on the desired transforming direction, corresponding valves are switched at a constant frequency in pulse-width mode. In order to keep the pressure ripples caused by the switching process in the output cavity C_O sufficiently low, the multiple parallel transformer stages are operated in a phase-shifted mode. Basically, the higher the number of parallel converter stages, the smaller the output cavity C_O can be. In the presented exemplary case, transformer stages are considered; however, the number is basically not restricted and depends on the requirements of the specific application, particularly, on the available components.

The digital transformer is designed for operation in all four power quadrants, as shown in Figure 8a. For convenience, the colors of the indicators $\mathcal{Q}_i$ match the colors of the switching valves in Figure 7, which are actuated for an operation in the corresponding power quadrant. If the supply pressure p_S is lower than the buffer pressure p_B and flow is delivered to the consumers ($q_S > 0$) , then the pressure is stepped down by actuating the valves V_B, which is defined as power quadrant $\mathcal{Q}_1$. In the reverse flow direction at the same pressure conditions and, thus, in power quadrant $\mathcal{Q}_2$, the pressure is boosted to the buffer pressure by switching valves V_T^B at constantly open valves V_S. When energy is recuperated, the DDP operates in idle mode and, thus, $q_P = 0$ and $q_B < 0$. In case of $p_S > p_B$, energy can be recuperated in power quadrant $\mathcal{Q}_3$ by stepping down the pressure to buffer pressure by switching valves V_S. Finally, in power quadrant $\mathcal{Q}_4$, the pressure is boosted by switching valves V_T^S at constantly open valves V_B. Since the buffer module is arranged in parallel with the DDP, the hydraulic output power can be boosted beyond the maximum motor power in the delivering operating area, at least to some extent, as illustrated in Figure 8b. Basically, boosting is an expensive operation because the flow through the inductance pipe must be accelerated by being connected to a tank for a corresponding amount of time and, thus, additional energy from the buffer must be spent. Furthermore, the boost performance also strongly depends on the size of the installed buffer accumulator.

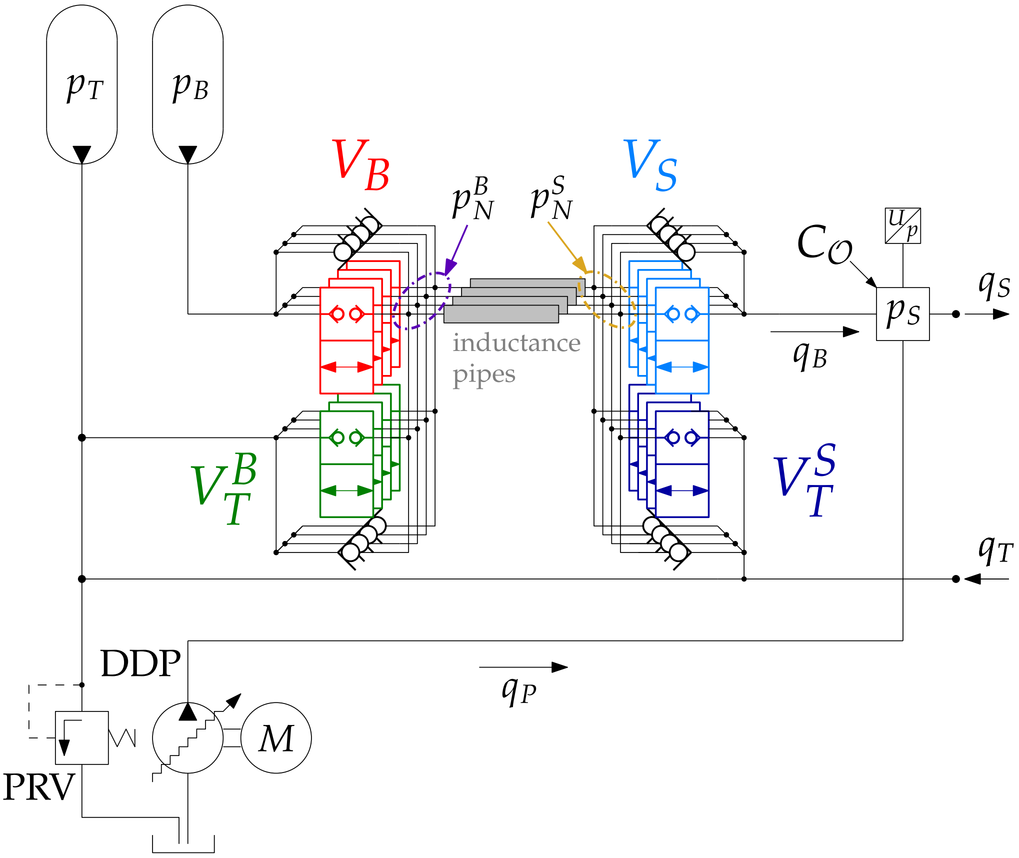

Figure 7. Load-sensitive supply unit with buffer module using a digital hydraulic transformer.

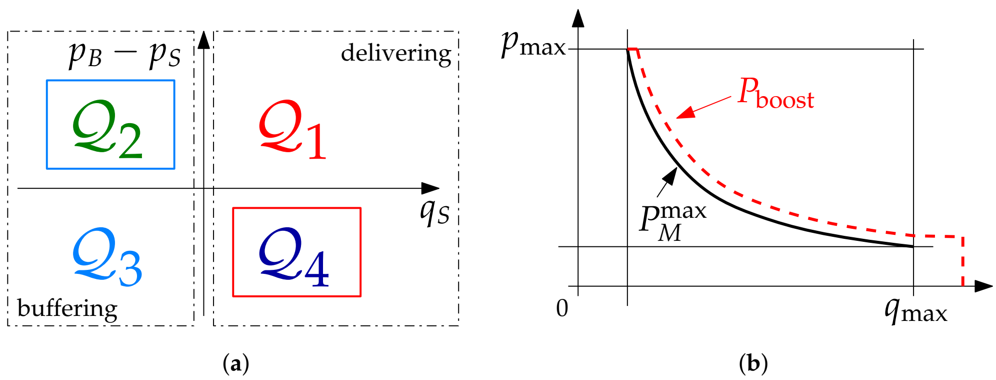

Figure 8. Operating areas of the DHT. (**a**) Power quadrants; (**b**) power range.

3. Simulations

The dynamic models of all investigated configurations are based on ordinary differential equations (ODEs) solved in *Python* using the method *solve_ivp* of the *scipy* package [28], which is a similar approach to that used to solve ODEs in *Matlab* with solvers like *ode23* or *ode45*. The overall simulation models of the investigated configurations would go beyond the scope of the contribution. But, for convenience, a dynamic mathematical model of one transformer stage is presented in the following.

The pressure build-up equation in one single node point of the DHT, as shown in Figure 7, reads

$$\dot{p}_N^X = \frac{E_{\mathcal{F}}}{V_N}\left(-q_{C_X^H} + q_{C_X^L} + q_{V_{X/T}^X} - q_{V_{X/T}^X} - q_{\text{pipe}}^X\right) \tag{1}$$

with $X \in \{B, S\}$, the compressibility modulus of the fluid $E_{\mathcal{F}} = 1.2e^9$ Pa and the volume of the node cavity $V_N = 0.05\,\ell$. The flow rate through one active switching valve calculates to

$$q_{V_{X/T}^X} = \xi_V Q_N^V \hat{\sqrt{\frac{\Delta p_{X/T}^X}{p_N}}} \tag{2}$$

with the actual pressure difference $\Delta p_{X/T}^X$, the valve opening ξ_V, the nominal flow rate Q_N^V, the nominal pressure drop p_N, and the orifice square-root characteristics

$$\hat{\sqrt{\cdot}} = \text{sign}(\cdot)\sqrt{|\cdot|}. \tag{3}$$

Furthermore, the switching valves have a specific switching time according to a rate-limited response. The indicator q_{pipe}^X represents the output flow rate at one port of the inductance pipe model, which is based on a transfer matrix incorporating linear wave propagation in the fluid and frequency-dependent friction according to [29]. The inputs of the pipe model are the pressures at both ends of the tube, p_N^X.

The flow rate through the check valves calculates to

$$q_{C_X^Y} = Q_N^C \Theta\left(\Delta p_X^Y\right) \hat{\sqrt{\frac{\Delta p_X^Y}{p_N}}} \tag{4}$$

with $Y \in \{H, L\}$, the actual pressure difference Δp_X^Y, the nominal flow rate Q_N^C, and $\Theta(\cdot)$ as the Heaviside function. The switching times of the check valves are neglected here, which is almost justified for plate check valves with response times below 1 ms.

3.1. Smart Actuator HBC052

The dynamic model of the cylinder actuator from Figure 3 is described by the ordinary differential equations

$$\dot{x}_P = v_P \tag{5}$$

$$\dot{v}_P = \frac{1}{m}(p_1 A_1 - p_2 A_2 - d_v v_P - F_P) \tag{6}$$

$$\dot{p}_1 = \frac{E_{\mathcal{F}}}{V_1^0 + A_1 x_P}(-A_1 v_P + q_1) \tag{7}$$

$$\dot{p}_2 = \frac{E_{\mathcal{F}}}{V_2^0 + A_2(l_C - x_P)}(A_2 v_P + q_2) \tag{8}$$

with the system parameters according to Table 1, including the dimensions of the DHT. The inputs are the load force F_P and the flow rates into both pressure chambers $q_{1/2}$ produced by the transformer clusters due to the duty ratios $\kappa_{1/2}$ according to the control scheme from Figure 4.

Table 1. Parameters of the HBC052.

piston sided cross-sectional area	$A_1 = \frac{63^2\pi}{4}\,\text{mm}^2$
rod sided cross-sectional area	$A_2 = \frac{(63^2-45^2)\pi}{4}\,\text{mm}^2$
full cylinder stroke	$l_C = 0.5\,\text{m}$
dead load	$m = 500\,\text{kg}$
viscous friction	$d_v = 0\,\frac{\text{Ns}}{\text{m}}$
switching valves	$Q_N^V = 10\,\ell/\text{min}@5\text{bar}$
response time switching valves	$t_S = 2\,\text{ms}$
check valves	$Q_N^C = 20\,\ell/\text{min}@5\text{bar}$
number of parallel switching converters	$n_{SC} = 4$
switching frequency	$f_S = 50\,\text{Hz}$
length of inductance pipe	$l_p = 1.5\,\text{m}$
diameter of inductance pipe	$d_p = 8\,\text{mm}$

Basically, the HBC052 actuator can be operated with a variable supply pressure, but for simplicity, in the following, only simulation results for a constant supply pressure of $p_S = 210\,\text{bar}$ are presented. In Figure 9, the simulation results for a ramp-like movement under a compressive and a tensile load force are also depicted; thus, an operation in all four power quadrants of the cylinder axis is presented. In Figure 9a, the tracking performance according to the control scheme from Figure 4 is illustrated. In the top diagram, the desired and the actual piston positions and, furthermore, the piston velocity are shown. In the first region, during an extending movement, a constant negative force, and, respectively, a tensile load force of $F_P = -10\,\text{kN}$ (see the upper diagram in Figure 9b) is applied to the piston rod, i.e., the actuator operates in braking mode. With regard to the control scheme from Figure 4, the piston sided pressure p_1 is controlled such that it is close to the tank pressure by the duty ratio κ_2 of the cluster mHBC$_2$, while the velocity is controlled by the duty ratio κ_1 of the cluster mHBC$_1$. At the simulation time of 1 s, the load force changes from a tensile to a considerably high compressive force, $F_P = 40\,\text{kN}$ (see upper diagram in Figure 9b), and the actuator switches from brake mode to drive mode. The fluctuations in the piston velocity result from the rapid change in the load force. In this phase, the PI-controller for the rod sided cluster mHBC$_2$ will to saturate ($\kappa_2 = -1$) from a certain force value, which represents an excitation of the closed-loop dynamics of the motion controller on the piston sided chamber. In order to get an impression of the energetic efficiency of the DHT, the viscous cylinder friction is completely neglected ($d_v = 0\,\frac{\text{Ns}}{\text{m}}$). Thus, the decay of the ripples in the velocity is mainly a result of losses due to the resistances of all valves (Q_N^X) of the DHT in combination with the empirically adjusted controller gain P_x, which, in turn, represents a compromise between stability and accuracy. In the considered application of an excavator, the dynamics of the desired trajectories are supposed to be much slower than the system dynamics and, thus, the response with a simple P-controller is acceptable. However, since the piston velocity is maintained by the cluster mHBC$_1$, only the pressure p_1 rises, while the rod sided pressure p_2 tends to tank pressure due to $\kappa_2 = -1$. In this phase, the converter cluster mHBC$_2$ does not switch any more, and the tank sided valves are constantly open. It must be remarked that the tracking performance during the change between braking and drive mode can be simply influenced by adjusting the controller parameters, which is not possible with common single-spool proportional valves suffering from fixed valve overlaps. Also, in common independent metering using proportional valves, this transition is often problematic, since at least two valves must fully switched at the same time, which often results in undesirable large ripples in the velocity. In the extending moving direction, the cluster $mHBC_2$ operates in boost mode, which means that a certain part of the downstream fluid from the rod sided chamber is directed to the supply line. In this specific case, this mode of operation does not represent a real recuperation, rather, it represents a regeneration, because the fluid harvested from the rod sided chamber is immediately reused in the piston sided chamber due to the extending movement. This can be observed in the middle diagram of Figure 9b in the simulation region $t = 0.5 \ldots 1$ s, where, even in brake mode, the actuator is consuming power; however, at a rate significantly less than the conventional hydraulic proportional drive (HPD).

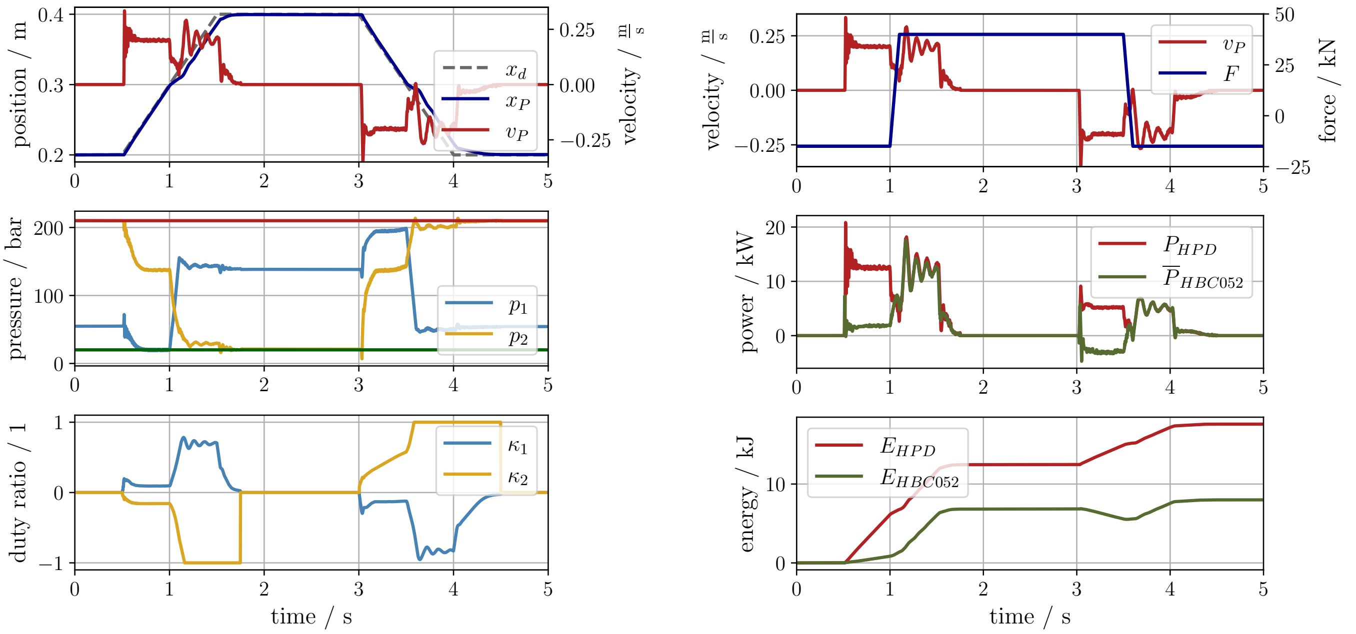

(**a**) (**b**)

Figure 9. Basic motion control of HBC052 in all power quadrants. (**a**) Tracking control; (**b**) energy consumption.

In the retracting direction, according to the control strategy (Figure 4), the pressure p_1 is controlled such that it is close to the supply pressure, and, thus, a real recuperation takes place, which can be seen in the bottom diagram of Figure 9b from simulation time $t = 3$ s, where the energy consumption of the digital hydraulic smart actuator (E_{HBC052}) and a conventional hydraulic proportional drive (E_{HPD}) are opposed. In this phase, the actuator feeds energy back into the supply system and the overall energy consumption decreases. Similar to the extending motion, now, the converter cluster $mHBC_2$ saturates to $\kappa_2 = 1$ when the tensile load force is applied again during the retracting moving direction. Like before, the oscillations in the velocity are excited by the rapid change in the load force and the saturation effect of the cluster $mHBC_2$. Since the cylinder friction is neglected, the transient of the closed-loop response decays with time according to the valve resistances in the DHT and the controller gain. It is remarkable that at the end of the simulation cycle, an energy saving in the range of 50% is achieved with the HBC052 axis compared to a conventional proportional drive.

3.2. Digital Hydraulic Supply Unit with Buffer Module

With regard to Figure 7, the mathematical model for the buffer accumulator reads

$$\dot{p}_B = \frac{E_o}{V_B\left(1 + \left(\frac{E_{\mathcal{F}}}{\varkappa p_B} - 1\right)\left(\frac{p_0^G}{p_B}\right)^{\frac{1}{\varkappa}}\right)}\left(\sum q_{V_B} + \sum q_{C_B^H}\right) \tag{9}$$

with the gas pre-load pressure p_0^G and the polytropic exponent $\varkappa \approx 1.3$. Furthermore, the pressure build-up equation in the output cavity of the supply unit calculates to

$$\dot{p}_S = \frac{E_{\mathcal{F}}}{C_{\mathcal{O}}}(q_B + q_P - q_S) \tag{10}$$

with the pump flow rate from the DDP $q_P\left(p_S^d, q_S\right)$ as a result from the P-controller for pressure control and $q_B = \sum q_{V_S}\left(p_S^d, q_S\right) + \sum q_{C_S^H}\left(p_S^d, q_S\right)$ being the flow rate resulting from the PWM actuation of the DHT according to a PI-controller. Thus, the remaining inputs are the actual load flow rate q_S and the desired supply pressure p_S^d in the LS-CPR demanded by the actuators.

For the presentation of the basic functionality of the buffer module with a DHT, an exemplary parameter set according to Table 2 is used, which is not related to a real application. In the presented simulation experiments, four parallel transformer stages were used, each switching at a frequency of 50 Hz in a phase-shifted pulse-width mode. For the used valve sizes and the inductance pipes, an empirically determined output cavity with a volume of 2 ℓ results in sufficiently low-pressure ripples at the node point $C_{\mathcal{O}}$. While the response time of the switching valves was considered with $t_S = 2\,\text{ms}$, the dynamics of the check valves was completely neglected, which can be nearly justified for plate check valves.

Table 2. Parameters of the DHT buffer module.

switching valves	$Q_N = 20\,\ell/\text{min}$@5bar
response time switching valves	$t_S = 2\,\text{ms}$
check valves	$Q_N = 40\,\ell/\text{min}$@5bar
number of parallel switching converters	$n_{SC} = 4$
switching frequency	$f_S = 50\,\text{Hz}$
length of inductance pipe	$l_p = 1.5\,\text{m}$
diameter of inductance pipe	$d_p = 8\,\text{mm}$
cavity at the output port	$C_{\mathcal{O}} = 2\,\ell$
buffer accumulator	$V_B = 5\,\ell$
pre-load pressure	$p_0^G = 40\,\text{bar}$
elevated tank pressure	$p_T = 10\,\text{bar}$

3.2.1. Modes of Operation

The first results show the basic operating areas of the DHT. In fact, the simulations were carried out with four parallel digital transformers; however, for clarity, in the following, the signals denoted with p_N^B and p_N^S in to Figure 7 represent the node pressures of only one selected transformer stage. In Figure 10, both power quadrants for energy recuperation ($q_B < 0$) are illustrated.

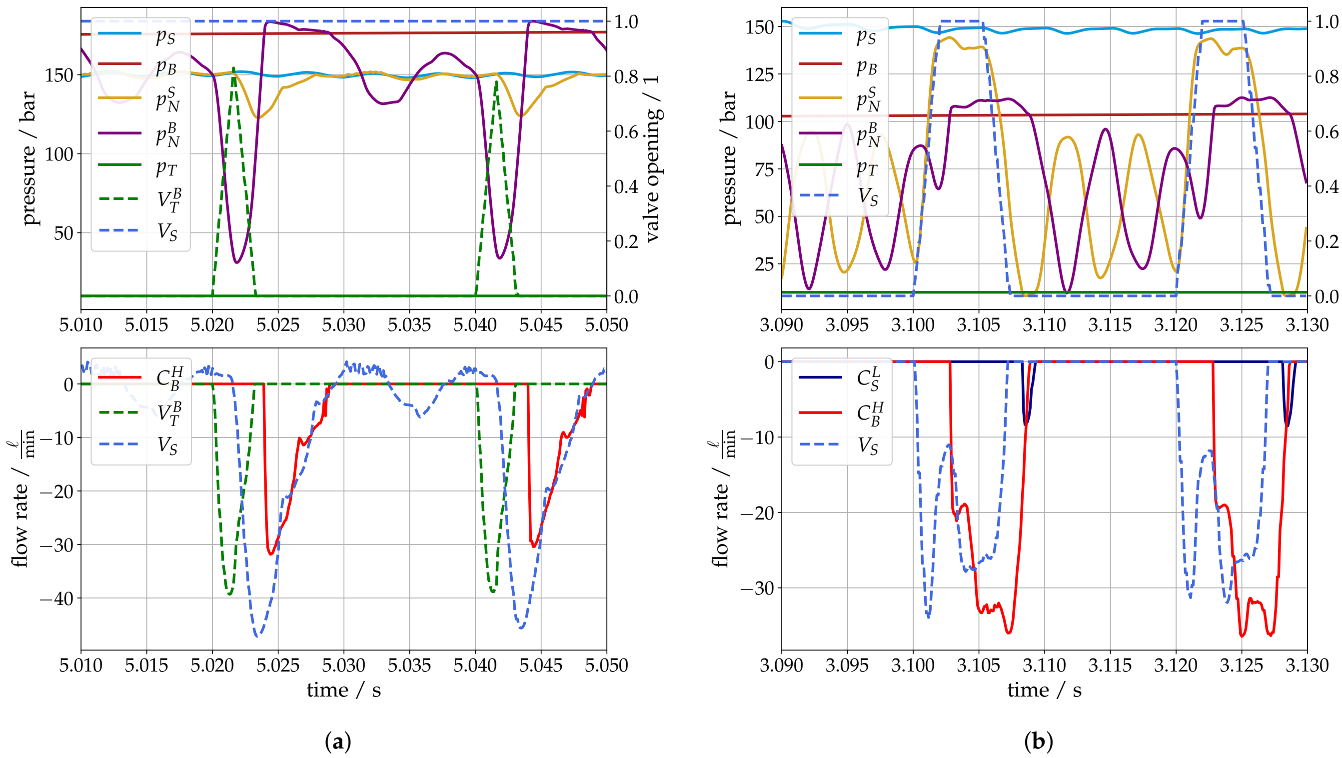

Figure 10. Energy recuperation ($q_B < 0$). (**a**) Power quadrant $\mathcal{Q}_2$ for $p_S < p_B$; (**b**) power quadrant $\mathcal{Q}_3$ for $p_S > p_B$.

In the upper diagram of Figure 10a, the buffer pressure p_B is higher than the supply pressure p_S; thus, the pressure is boosted as a result of the spill-over of kinetic energy in the inductance pipe. For this purpose, the flow through the inductance pipe must be accelerated by pulsing the valve V_T^B while the supply sided valve V_S is constantly open. When the valve V_T^B is shut quickly, then the spill-over of the kinetic energy in the inductance pipe causes the pressure p_N^B to overshoot the buffer pressure p_B, resulting in a flow through the buffer sided high-pressure check valve C_B^H, which is illustrated in the lower diagram. The fluctuations in the node pressures p_N^B and p_N^S result from wave propagation effects in the inertance pipe due to the rapid PWM switching of the valves. In the second recuperative case depicted in Figure 10b, the buffer pressure p_B is lower than the supply pressure p_S, and, thus, the pressure is stepped down for energy recuperation by pulsing the valve V_S for an acceleration of the flow through the inductance pipe. In this specific case, the actual ratio between p_B and p_S results in a reduced spill-over effect, and, thus, only a smaller amount of fluid is drawn from the tank through the supply sided low-pressure check valve C_S^L. Therefrom, this example emphasizes that recuperation of energy is also associated with efficiency, which always depends on the actual operating conditions. Furthermore, in such an operating case, i.e., when fluid is only marginally drawn from the tank, then a stronger excitation of the resonator comprising both node volumes and the pipe inductance is present. This can be nicely identified by the 180° phase shift of both node pressure signals, p_N^B and p_N^S, during the off period of the switching valve V_S.

In Figure 11, the power quadrants for releasing the stored energy from the buffer accumulator to the LS-CPR are illustrated.

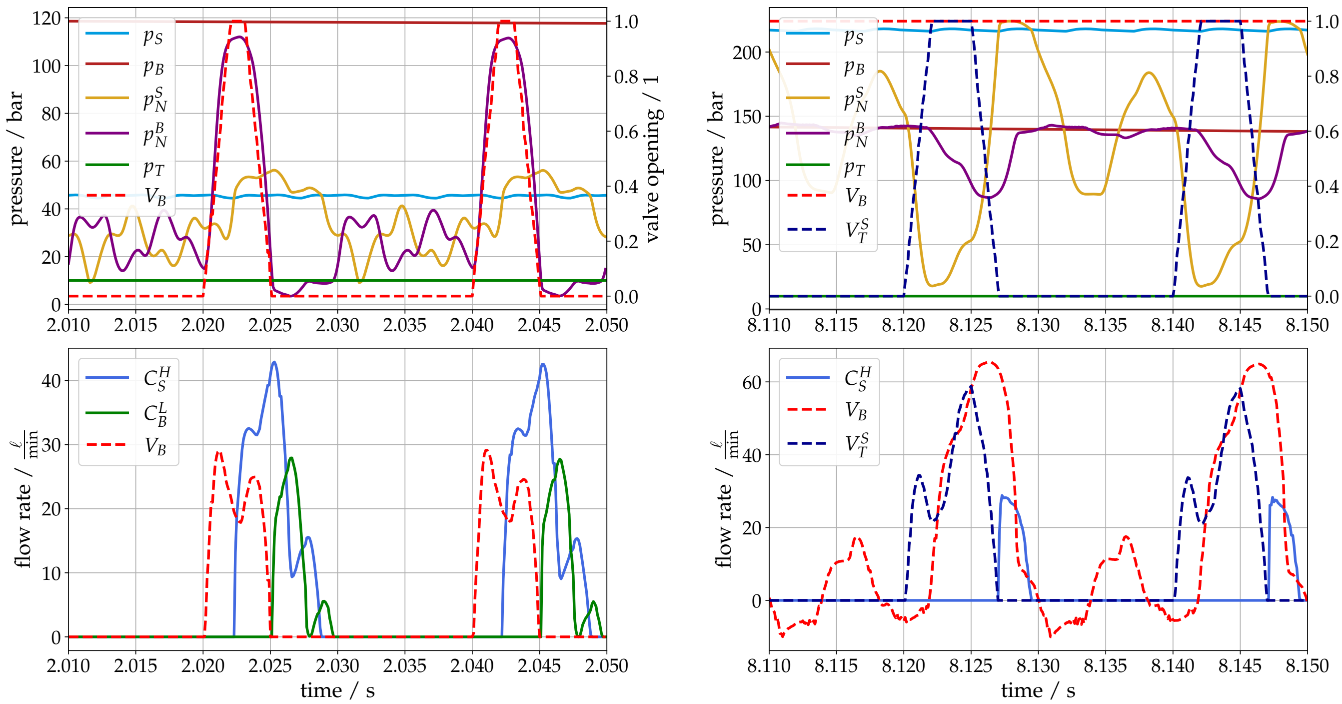

Figure 11. Releasing energy from the buffer ($q_B > 0$). (**a**) Power quadrant $\mathcal{Q}_1$ for $p_S < p_B$; (**b**) power quadrant $\mathcal{Q}_4$ for $p_S > p_B$.

Figure 11a shows an efficient pressure step-down operation. In the upper diagram, the pressure signals and the valve opening of the actively switched valve V_B for acceleration of the flow in the inductance pipe are illustrated. By shutting valve V_B quickly, the spill-over of kinetic energy forces the pressure p_N^B to fall below the tank pressure and results in a flow rate of C_B^L from the tank, as depicted in the lower diagram. The flow rate C_S^H through the high-pressure check valve on the supply side results from the elevated node pressure p_N^S above the supply pressure p_S. Thus, in this case, the buffer pressure is stepped down and the flow is boosted.

The final operating case shown in Figure 11b represents a pressure boost to the LS-CPR, which may result in a power boost, if the primary motor operates at its maximum power. In this case, the valve V_B is constantly open and the valve V_T^S has to be switched in pulse-width mode.

3.2.2. Simulation of a Basic Working Cycle

In the following, a short exemplary working cycle for the demonstration of all four power quadrants is investigated by simulation. For this purpose, a parameter set for the primary hydraulic supply comprising the motor and the digital displacement pump according to Table 3 is considered. Since only the energetic performance of the buffer module is the focus of the investigations, the pump and the motor are considered to be ideal with regard to efficiency.

Table 3. Parameters of the primary hydraulic supply.

Motor		DDP	
maximum power	$P_M^{\max} = 20\,\text{kW}$	number of pistons	12
rotational speed	$n_P = 2000\,\text{rpm}$	total displacement volume	$V_D = 96\,\text{cm}^3$

At first, the simulation results for the working cycle only with the motor/DDP combination and without the buffer module are shown in Figure 12. The upper diagram shows the response of the DDP as a stepwise profile of the supply pressure p_S according to the load flow rate q_S depicted in the lower diagram. When the load flow rate $q_S < 0$, then the pump flow rate q_P is truncated to zero and, thus, the DDP is forced to idle mode, since no energy can be recuperated with the used motor/DDP combination. The peaks in the pump flow rate indicate the additional flow, which is necessary for raising the pressure in the output cavity, i.e., for compression of the fluid. Basically, the remaining control error in the pressure results from using a simple P-controller for tracking. But, at the simulation time $t = 8\,\mathrm{s}$, the power required by the load exceeds the maximum power of the motor and, thus, the desired pressure cannot be realized before the load flow rate is lowered at time $t = 8.5\,\mathrm{s}$.

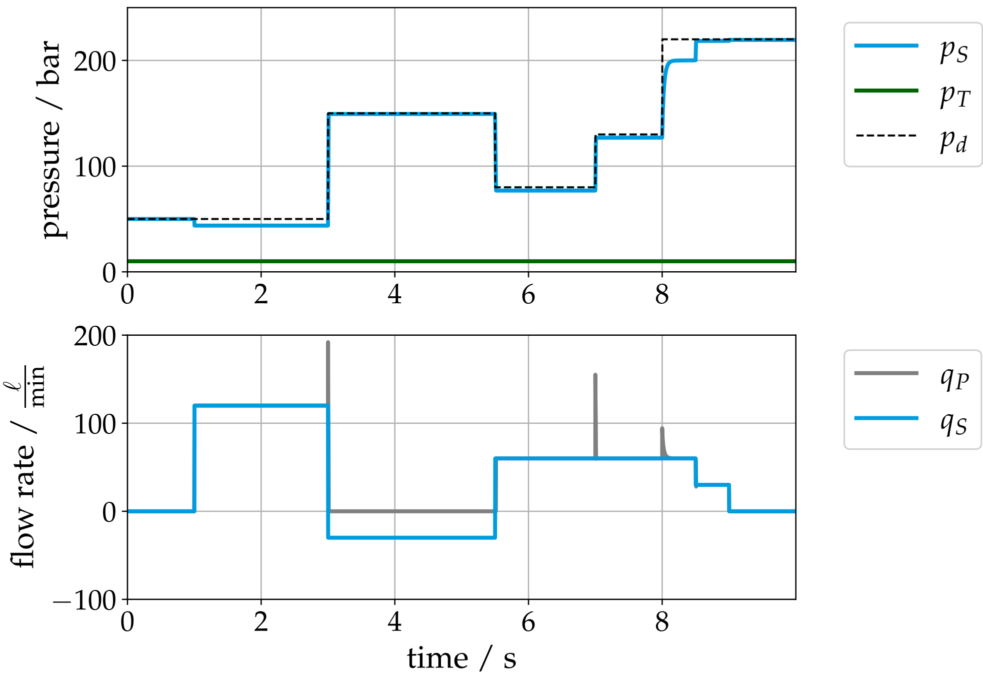

Figure 12. Working cycle with the motor/DDP configuration.

The simulation results for the same working cycle with the DDP plus the buffer module using a DHT are presented in Figure 13. Similar to above, in the upper diagram, the pressure responses are illustrated. The DHT is controlled with a simple and empirically parameterized PI-controller. At the beginning of the working cycle, the initial pressure of the buffer accumulator is $p_B = 150\,\mathrm{bar}$ and the desired supply pressure is 50 bar. When the first step in the load flow rate q_S occurs, both the DDP and the DHT start to deliver flow, which is indicated by the signals q_P and q_B. The buffer operates in $\mathcal{Q}_1$, which is illustrated by the dashed line in the additional axis for the actual power quadrant in the lower diagram. Like in Section 3.2.1, the signals p_N^B and p_N^S indicate the pressure in the buffer sided node points and in the supply sided node points of one transformer stage. When p_N^B falls below tank pressure during $\mathcal{Q}_1$, then energy is efficiently released from the buffer by boosting the flow with cheap oil from tank. A similar scenario is valid for p_N^S, when the operating mode changes at simulation $t = 3\,\mathrm{s}$, where a high supply pressure of $p_S = 150\,\mathrm{bar}$ and a negative load flow rate are required, for instance, due to picking up a heavy load for lowering. The power quadrant switches to $\mathcal{Q}_3$ since the buffer pressure is lower than the supply pressure. The total flow q_B is used to load the buffer accumulator. When the buffer pressure exceeds the supply pressure, the operating mode of the DHT changes to power quadrant $\mathcal{Q}_2$ for pressure boosting of p_B. In this mode of operation, a certain amount of q_B must be used for boosting the pressure and only a reduced flow rate can be stored in the buffer. At $t = 5\,\text{s}$, the conditions of the working cycle require an operation again in $\mathcal{Q}_1$ and energy from the buffer is released efficiently, again by boosting a certain amount of fluid from tank pressure to supply pressure.

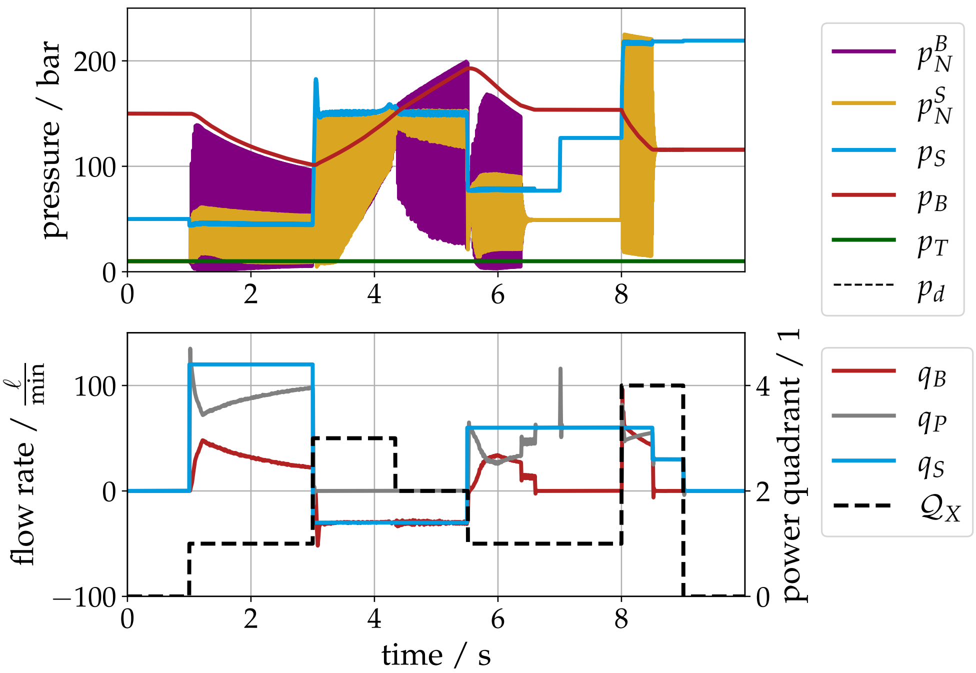

Figure 13. Supply performance with the buffer module using the DHT.

In certain situations, it can be advantageous to deactivate the buffer module, which is easily possible due to the parallel arrangement with the primary hydraulic supply. For instance, at simulation time $t \approx 6.5\,\text{s}$, the buffer module is switched off, because in the following operating conditions, the energy from the buffer could only be transformed with additional throttling losses. Thus, the energy in the buffer can be either stored until the operating conditions allow an efficient exploitation or can be saved up for a predictable power boost, like that occurring at simulation time $t = 8\,\text{s}$. In this situation, the desired power exceeds the maximum power of the primary motor, as already shown in Figure 12, but with the additional power of the buffer module, the desired pressure can be realized for the demanded load flow rate.

In Figure 14, the power and the energy consumption of the DDP without and with the buffer module are presented.

In the upper diagrams, the power consumption, and in the lower diagrams, the energy consumption for the considered working cycle are illustrated. Until the simulation time $t = 8\,\text{s}$, the desired output power is within the designated working range of the motor and the deviations result from the simple P-controller used for the DDP in the simulation experiments. But in this time range, the results can be directly compared, because as already mentioned, from $t = 8\,\text{s}$, the desired power at the output exceeds the maximum power of the motor. Thus, at $t = 8\,\text{s}$, the energy consumption of the DDP without the buffer module is approximately 42 kJ, which is depicted in the lower diagram of Figure 14a. In the corresponding results with the buffer module, depicted in Figure 14b, the energy consumed by the pump reads 35 kJ, which is significantly lower due to the buffering and releasing of recuperable energy from the load cycle. Since the red signal representing the energy contribution of the buffer is almost zero at time $t = 8$ s, the reduced energy consumption can be directly interpreted as energy savings at the motor and, thus, of primary energy.

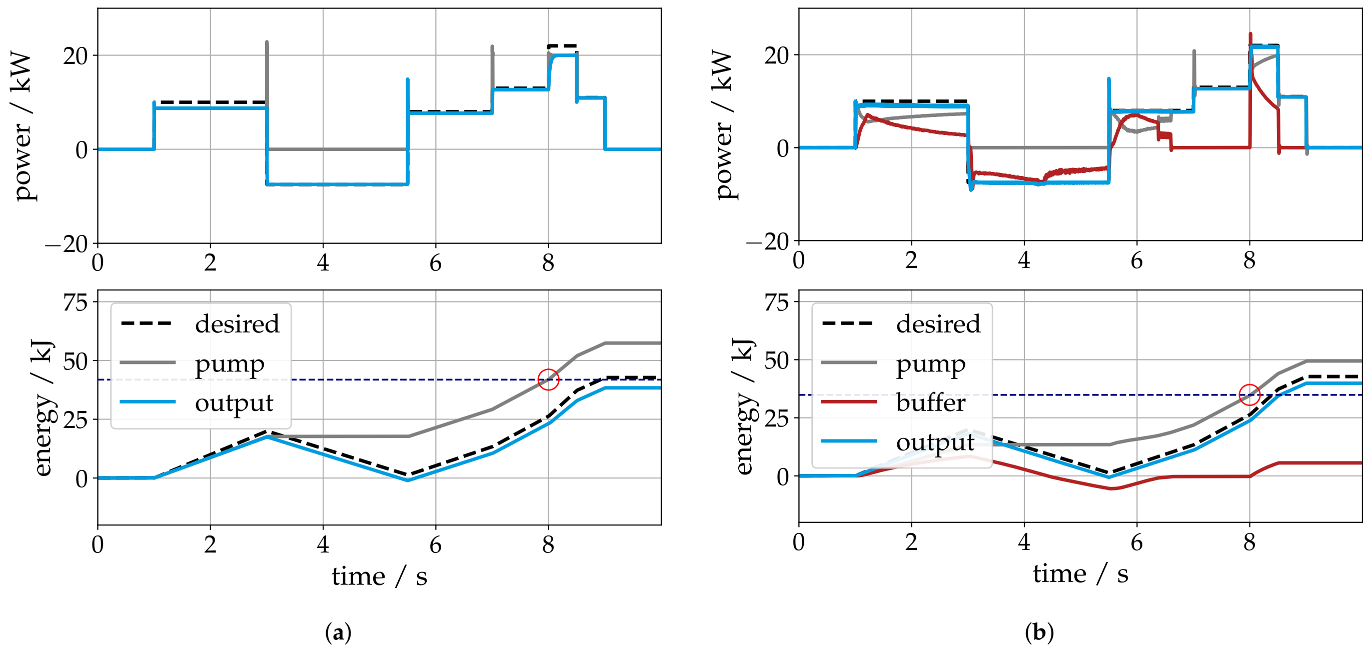

Figure 14. Power consumption. (**a**) DDP without buffer module; (**b**) DDP with buffer module and DHT.

As already mentioned, in Figure 14b, from $t = 8$ s, the output power is boosted above the maximum power of the motor for a short time, for instance, for an acceleration of a very heavy load. Therefore, a significant amount of energy is used from the buffer module; however, for the whole working cycle, the output performance as well as the total energy consumption, including the buffer module, could be lowered by using recuperable energy from the load.

3.2.3. A More Realistic Working Cycle

The working cycle presented in previous section was quite academic; however, the basic concept and principles of operation could be shown. In this section, the tracking performance of the supply pressure p_S and ability of buffering energy provided by the load is investigated for the trench-digging cycle from Figure 2b. In particular, the signals q_S, as the load flow rate in the LS-CPR, and p_S, as the desired pressure p_S^d, are used as input signals for the overall simulation model. In fact, trench digging is a power-demanding operation, and, consequently, only a small amount of recuperable energy is available. For this reason, only a specific section from time $t = 20 \ldots 30$ s of the full trench-digging cycle from Figure 2b is investigated. At first, in Figure 15, the simulation results for the primary supply unit, particularly, the motor/DDP configuration, are presented for the mentioned section of the working cycle.

The spikes in pressure and velocity between $t = 20$ s and 22 s are not discussed, because the corresponding power consumption results from the switching of the force directional valves of the actuator and, thus, it is not the focus of this investigation. Much more interesting is the short phase, where the flow rate is becoming negative, which implies a negative, particularly, a recuperative power. The primary hydraulic supply, consisting only of motor and DDP, is not able to recuperate and, thus, the configuration is not able to follow the desired pressure trajectory p_d, because the DDP is only able to reduce the flow to zero due to the constantly rotating motor. Furthermore, at simulation times $t = 26$ s and

$t \approx 27\,\mathrm{s}$, some fluctuations in the actual pressure signal p_S can be observed. This behavior is a result of the power limitation of the primary motor, which can be explained by Figure 16, where the desired power overshoots the maximum power, $P_{\max}$, of the primary motor.

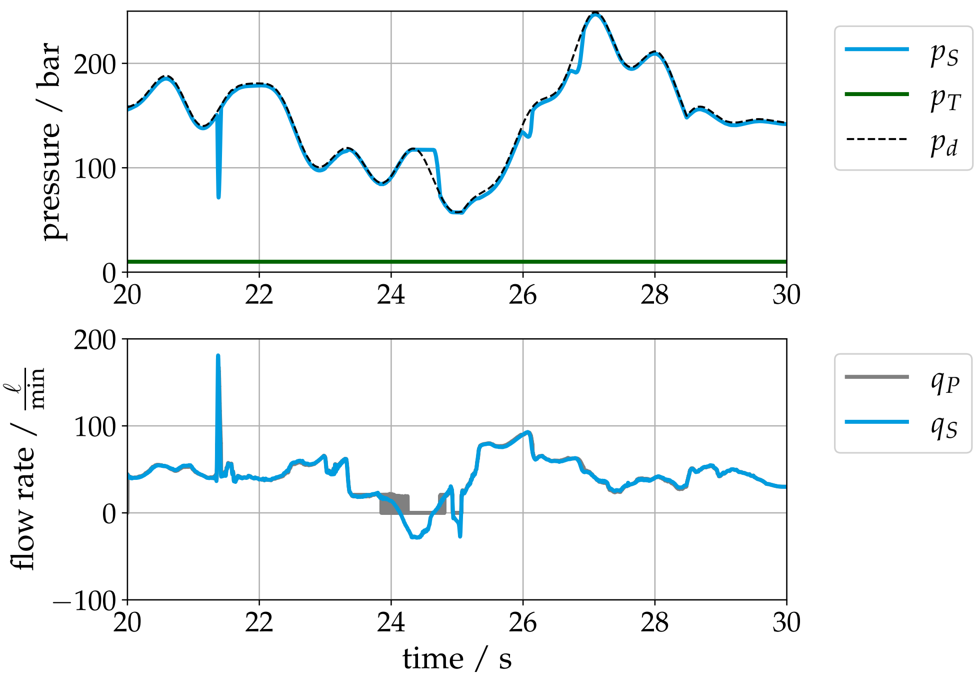

Figure 15. Trench-digging cycle with the motor/DDP configuration.

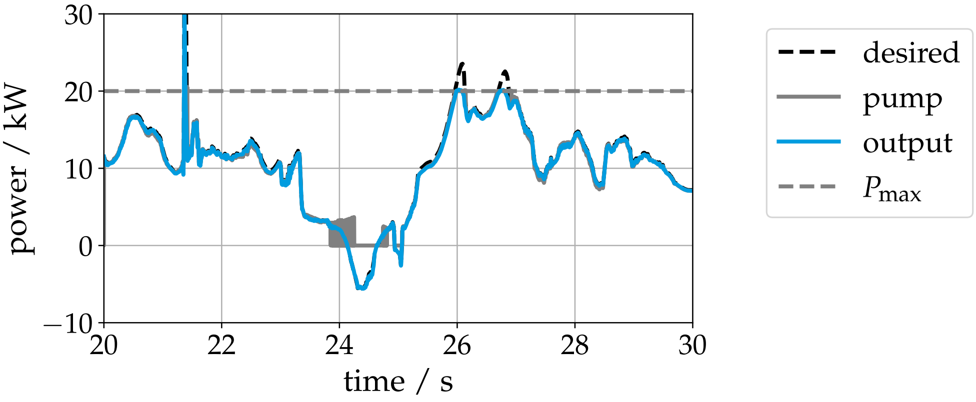

Figure 16. Power consumption for trench digging with DDP.

In Figure 17, the simulation results for the same section of the trench-digging cycle with the digital hydraulic buffer module installed in parallel with the DDP are presented.

Again, in the upper diagram, the pressure signals are plotted, and, in the lower diagram, additionally, the flow rates and the power quadrants of the DHT are indicated. It can be seen that most of the time, the DDP is able to maintain the demanded power, which is indicated by the nearly constant buffer pressure p_B. Thus, the controller output of the buffer module, i.e., the duty ratio of the DHT, is almost zero, and nearly no switching is observable due to the dynamics of the valves. At simulation time $t = 24\,\mathrm{s}$, the recuperation phase starts, and from this point on, the DHT boosts the buffer pressure p_B, and, thus, energy is stored in the accumulator. The next points of interest are the phases when the power consumption exceeds the maximum power of the motor, which takes place at simulation times $t = 26\,\mathrm{s}$ and $t \approx 27\,\mathrm{s}$. Here, the DHT operates in power quadrant $\mathcal{Q}_X = 4$, which means boosting from buffer pressure p_B to the supply pressure level p_S as long the power of the primary motor is in saturation. Thus, with the parallel arrangement of the DDP and the buffer module, the tracking of the desired supply pressure p_d can be easily maintained. Moreover, the mentioned sharp spike in the power consumption due to the switching of the force directional (FD) valves of the previous actuator concept can be nearly compensated due to the very short response time of the DHT, according to the fast valve switching, within a few milliseconds. In order to round off the presentation of the results, the power consumption for the trench digging with the DHT is illustrated in Figure 18.

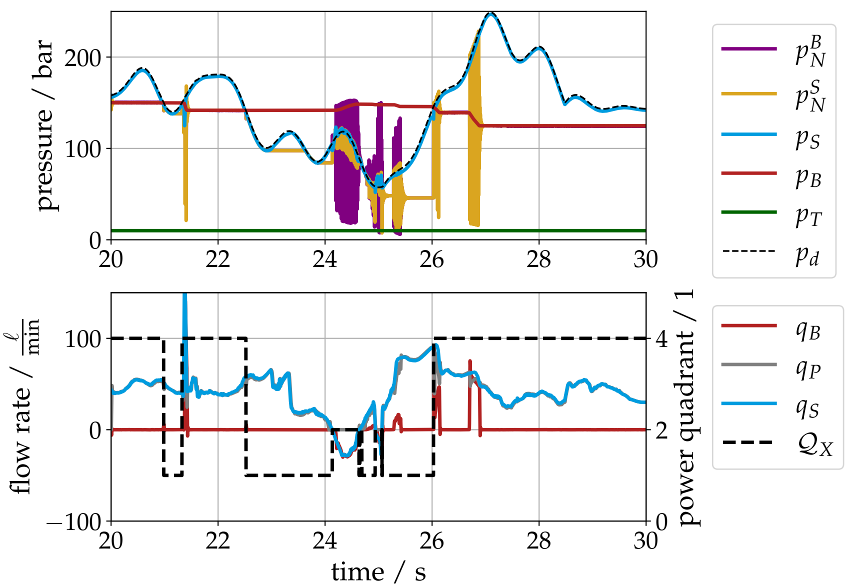

Figure 17. Supply performance for the trench-digging cycle with the buffer module using the DHT.

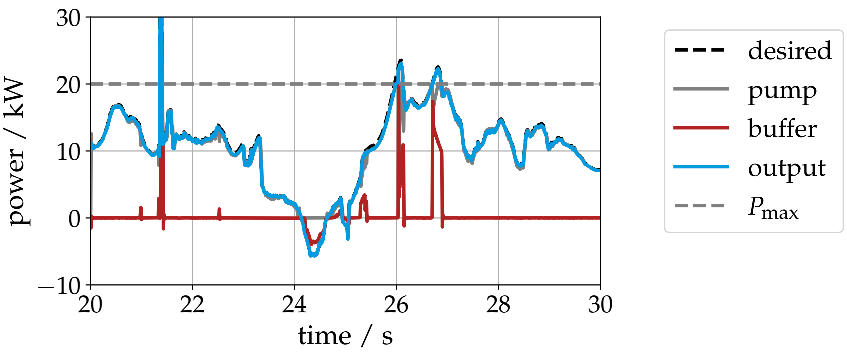

Figure 18. Power consumption for the digging of a trench with a DHT.

4. Discussion

4.1. Limitations of the Simulation Models

This study is based on simulation experiments; therefore, it is important to reflect on the reliability of the results. The differential equations of most models, like, for instance, momentum equations or valve orifice equations, are well established and are classified as reliable. For pressure build-up equations in cavities and cylinder chambers, a constant compressibility modulus is assumed, which is justified at moderate pressure rates as it is the case in the simulation experiments. The most uncertainty is given by the dynamic model of the inductance pipe, which assumes laminar flow conditions. In certain phases of a periodic switching cycle, a transition to turbulent flow and, thus, increased losses cannot be ruled out; however, measurements with previous prototypes showed an acceptable agreement with the simulation models, at least with straight pipe lines. For a compact design of the transformer, the pipes must be coiled in a certain way, and, thus, additional losses must be expected, which may lead to a considerable reduction in the efficiency of the DHT, if the mechanical design and, thus, the realization of the coiling is inappropriate. This uncertainty is the main reason for avoiding too many quantitative indicators regarding efficiency from the simulation results in this contribution.

4.2. Smart Actuator HBC052

Compared to the HERCULES actuator from [15], the advanced prototype HBC052 benefits from the independent converter stages for each flow direction and pressure chamber. Even in cases of an instantaneous change of the power quadrants, a satisfying tracking can be achieved with simple control strategies. Furthermore, due to the decoupling of the stages from the moving directions, the number of switching cycles of the high dynamic valves is significantly reduced and an extended lifetime may be expected. However, a higher number of high dynamic valves is necessary, which may increase the costs of such an actuator, but on the other hand, the component variety necessary for a realization is reduced. Even though in this contribution, only simulation results for a basic working cycle could be presented, nonetheless, a significant reduction in the energy consumption seems to be possible over a wide operating range.

In the use case of an excavator, the smart actuators are supplied by a load-sensitive common pressure rail (LS-CPR). This means that recovered fluid from one actuator can be immediately reused by another actuator, which, in turn, reduces the consumption of primary energy. Furthermore, since all valves for motion control are located directly at the actuators, only one LS-CPR and one tank line must be installed along the arm of the excavator, and, thus, the overall piping effort can be reduced significantly, which in turn lowers the installation costs.

4.3. Supply Unit with Buffer Module and DHT

The concept of an efficient load-sensitive hydraulic power supply is represented by a parallel arrangement of a DDP and a digital hydraulic transformer connected to a buffer accumulator. Basically, the concept is not limited to a realization with a DDP; all other adjustable pumps would be also possible. The DDP was chosen as an example of a highly efficient method for controlling the flow. For simplicity, in this contribution, the DDP is driven by a motor with a constant rotational speed, which allows a very energy-efficient and cost-effective realization of the primary hydraulic supply. However, in a probably more sophisticated approach, a motor with a variable speed can also be included into the optimization process to minimize the energy consumption at maximum performance, or furthermore, different optimization objectives depending on specific operating conditions can even be considered. Nevertheless, the effectiveness of the presented buffer concept strongly depends on the actual operating conditions, particularly the working cycles of the machine; in other words, recuperable energy must be available.

In the presented study, the output pressure is controlled, which requires a specific desired value of p_S ,which, in turn, must be generated by a certain strategy involving the demand of all individual consumers located in the LS-CPR. For this reason, the concept is not easily comparable with conventional load-sensing systems, like open-center or closed-center systems. However, the presented concept does not suffer from any piloting or sensing losses. Furthermore, the hydraulic buffer module is preferably suitable for drive-by-wire applications with smart actuators, which already fulfill the requirements for energy recuperation, like, for instance, independent metering.

The digital hydraulic transformer (DHT) represents a highly efficient valve-controlled system using an inertance pipe for transforming the hydraulic power. However, in the transformer, certain losses due to parasitic effects, like limited valve sizes, flow losses in the pipe, or compression losses in the transformer nodes have to be considered. For instance, the step-down efficiency is rather high at lower output pressures, because in such an operating case, much fluid can be drawn from the tank line. But, since the buffer module is arranged in parallel with the primary hydraulic supply, the buffer module may be deactivated at operating points with lower efficiency. Thus, recuperation as well as the release of energy can be either suspended or forced in certain situations. Furthermore, if there exist some predictable operating points with extreme power consumption, the energy in the buffer can be saved up and used on demand. Moreover, it is conceivable to load the buffer accumulator directly by the pump through an additional (not illustrated) bypass during phases of low output power in order to have a higher pressure reserve for power boosting.

In mobile applications, for which the presented concept will most likely be beneficial, the space for additional devices is hardly available. But, if only smart actuators are used in the LS-CPR, then all valves are located close to or directly in the actuator. Thus, new room is generated in the body of the machine, which can be used for the buffer module. In particular, space for the accumulator, the DHT, and the output cavity must be made. The size of the accumulator strongly depends on the strategy of operation: buffering, saving, or even, preferably, boosting. The space required for the DHT depends strongly on the mechanical design. Based on the results from [15], a compact design seems to be possible, where the switching valves and the check valves can be integrated in a single block incorporating coiled or threaded inductances around the output cavity, which in turn may result in a minimized amount of required space.

Finally, the noise due to the valve switching of the DHT has not been investigated so far; however, it can be assumed that the IHT also suffers from considerable noise during transforming hydraulic power. But the multiple transformer stages of the DHT constitute additional degrees of freedom by adapting the number of active stages as well as the switching frequency in order to minimize the noise emissions during operation.

5. Conclusions

The demand for more efficient hydraulic drives requires more efficient hydraulic actuators, and supply units as well. In fact, throttling losses can be reduced by the application of load-sensing systems; however, conventional drive systems are not able to recuperate energy. In this paper, an improved smart actuator and the concept of a buffer module for storing recuperable energy using digital hydraulic transformers based on a PWM switching technique were presented. The basic operation in all four power quadrants has been demonstrated by simulation experiments. The investigated use cases were related to an excavator arm with multiple smart actuators supplied by one load-sensitive common pressure rail. The results show that compared to traditional concepts, like proportional valve control and conventional load sensing, the energy consumption in exemplary operating cycles could be reduced significantly by the use of smart actuators and a pressure supply with a buffer module. Both concepts benefit from the ability to transform recuperable energy provided by the load, which offers new perspectives for energy-efficient motion control. Furthermore, during driving operations, the energy stored in the buffer accumulator can be efficiently added to the primary supply unit, resulting in a power boosting beyond the maximum power of the primary motor to some extent, which, in turn, provides room for the downsizing of primary supply units in some applications. In the presented study of an excavator arm during trenching, the results showed an excellent performance in controlling the pressure in the load-sensitive common pressure rail with simple control strategies. The next steps in the development are advanced investigations of the presented smart actuator in combination with the efficient supply unit in more specific working cycles, for the present by simulation. Furthermore, an extended simulation study for a whole excavator arm incorporating multiple smart actuators supplied by a DDP with a buffer module would make sense. Then, certainly, a study with real prototypes would be desirable.

Funding: This work has been supported by the COMET-K2 Center "Center for Symbiotic Mechatronics" of the Linz Center of Mechatronics (LCM), funded by the Austrian federal government and the federal state of Upper Austria.

Data Availability Statement: The data presented in this study are available on request from the corresponding author.

Conflicts of Interest: The author declares that the research was conducted in the absence of any commercial or financial relationships that could be construed as a potential conflict of interest.

Abbreviations

The following abbreviations are used in this manuscript:

CPR	common pressure rail
DDP	digital displacement pump
DHT	digital hydraulic transformer
FD	force direction
HBC	hydraulic buck converter
HPD	hydraulic proportional drive
IHT	INNAS Hydraulic Transformer
LS	load sensing
LS-CPR	load-sensitive common pressure rail
ODEs	ordinary differential equations
PRV	pressure relief valve
VD	velocity direction

References

1. Heybroek, K.; Larsson, J.; Palmberg, J.O. The Potential of Energy Recuperation in Valve Controlled Mobile Hydraulic Systems. In Proceedings of the 11th Scandinavian International Converence on Fluid Power (SICFP'09), Linköping, Sweden, 2–4 June 2009.
2. Vukovic, M.; Leifeld, R.; Murrenhoff, H. Reducing Fuel Consumption in Hydraulic Excavators—A Comprehensive Analysis. *Energies* **2017**, *10*, 687. [CrossRef]
3. Abuowda, K.; Okhotnikov, I.; Noroozi, S.; Godfrey, P.; Dupac, M. A review of electrohydraulic independent metering technology. *ISA Trans.* **2020**, *98*, 364–381. [CrossRef]
4. Ahamad, M.; Dinh, Q.T.; Nahian, S.A.; Ahn, K.K. Development of a New Generation of Independent Metering Valve Circuit for Hydraulic Boom Cylinder Control. *Int. J. Autom. Technol.* **2015**, *9*, 143–152. [CrossRef]
5. Choi, K.; Seo, J.; Nam, Y.; Kim, K.U. Energy-saving in excavators with application of independent metering valve. *J. Mech. Sci. Technol.* **2015**, *29*, 387–395. [CrossRef]
6. Huova, M.; Tammisto, J.; Linjama, M. Open-loop Independent Metering Control of a Multi-DOF Forwarder Boom. *Int. J. Fluid Power* **2020**, *21*, 147–168. [CrossRef]
7. Ketonen, M.; Linjama, M. Digital Hydraulic IMV System in an Excavator—First Results. In Proceedings of the 16th Scandinavian International Conference on Fluid Power (SICFP'19), Tampere, Finland, 22–24 May 2019.
8. Achten, P. Fundamentals of Hydraulic Transformers. In Proceedings of the 14th International Fluid Power Conference IFK, Dresden, Germany, 19–21 March 2024.
9. Negri, V.J.D.; Wang, P.; Plummer, A.; Johnston, N.D. Behavioural Prediction of Hydraulic Step-Up Switching Converters. *Int. J. Fluid Power* **2014**, *15*, 1–9. [CrossRef]
10. Yuan, C.; Pan, M.; Plummer, A. A Review of Switched Inertance Hydraulic Converter Technology. *J. Dyn. Syst. Meas. Control* **2020**, *142*, 050801. [CrossRef]
11. Wang, F.; Gu, L.; Chen, Y. A continuously variable hydraulic pressure converter based on high-speed on-off valves. *Mechatronics* **2011**, *21*, 1298–1308. [CrossRef]

12. De Negri, V.J.; Nostrani, M.P.; Wang, P.; Johnston, D.N.; Plummer, A. Modelling and analysis of hydraulic step-down switching converters. *Int. J. Fluid Power* **2015**, *16*, 111–121. [CrossRef]
13. Pan, M.; Plummer, A. Digital switched hydraulics. *Front. Mech. Eng.* **2018**, *13*, 225–231. [CrossRef]
14. Chen, X.; Zhu, Y.; Wiens, T.; Bitner, D.; Ling, J. Characteristic investigation of a flow-dependent inertia hydraulic converter driven by an equivalent fast switching valve. *Proc. Inst. Mech. Eng. Part C J. Mech. Eng. Sci.* **2022**, *236*, 3354–3374. [CrossRef]
15. Kogler, H.; Scheidl, R.; Lauber, M.; Winkler, B. Hydraulic Efficient and Robust Converter Unit for Linear Motion under Energy Saving. In Proceedings of the 11th Workshop on Digital Fluid Power 2022, Edinburgh, UK, 19–20 September 2022.
16. Qin, Y.; Yang, Y.; Li, S.; Huang, Y.; Tan, S.C.; Hui, S.Y. A High-Efficiency DC/DC Converter for High-Voltage-Gain, High-Current Applications. *IEEE J. Emerg. Sel. Top. Power Electron.* **2020**, *8*, 2812–2823. [CrossRef]
17. Duan, J.; Wang, S.; Xu, Y.; Fan, S.; Zhao, K.; Sun, L. Variable Multiple Interleaved Bi-Directional DC/DC Converter with Current Ripple Optimization. *Appl. Sci.* **2023**, *13*, 1744. [CrossRef]
18. Vael, G.E.M.; Achten, P.A.J.; Fu, Z. *The Innas Hydraulic Transformer The Key to the Hydrostatic Common Pressure Rail*; SAE Technical Paper; SAE International: Warrendale, PA, USA, 2000. [CrossRef]
19. Achten, P.; Potma, J.; Achten, S.; Achten, J.; Mommers, R. The Design of the FCT80 Hydraulic Transformer. In Proceedings of the 18th Scandinavian International Conference on Fluid Power (SICFP'23), Tampere, Finland, 30 May–1 June 2023.
20. Vael, G.; Orlando, E.; Stukenbrock, R. Toward Maximum Flexibilty in Working Machinery, IHT Control in a Mecalac Excavator. In Proccedings of the 4th International Fluid Power Conference, Dresden, Germany, 19–21 March 2024; pp. 171–182.
21. Casoli, P.; Riccò, L.; Campanini, F.; Bedotti, A. Hydraulic Hybrid Excavator—Mathematical Model Validation and Energy Analysis. *Energies* **2016**, *9*, 1002. [CrossRef]
22. Wang, J.; Yang, Z.; Liu, S.; Zhang, Q.; Han, Y. A comprehensive overview of hybrid construction machinery. *Adv. Mech. Eng.* **2016**, *8*, 1687814016636809. [CrossRef]
23. Kogler, H. Efficient and Load Sensitive Hydraulic Supply Unit using Multiple Switching Converters. In Proceedings of the Twelfth Workshop on Digital Fluid Power (DFP24), Tampere, Finland, 6–7 June 2024.
24. Linjama, M.; Uusi-Heikkilä, J. (Eds.) *The Twelfth Workshop on Digital Fluid Power, DFP24*; Tampere University: Tampere, Finland, 2024.
25. Rampen, W.H.S. Digital Displacement Hydraulic Piston Pump. Ph.D. Thesis, The University of Edinburgh, Edinburgh, UK, 1992.
26. Williamson, C.; Manring, N. A More Accurate Definition of Mechanical and Volumentric Efficiency for Digital Displacement Pumps. In Proceedings of the ASME/BATH 2019 Symposium on Fluid Power and Motion Control (FPMC 2019), Sarasota, FL, USA, 7–9 October 2019.
27. Pellegri, M.; Green, M.; Macpherson, J.; McKay, C.; Caldwell, N. Applying a multi-service digital displacement® pump to an excavator to reduce valve losses. In Proceedings of the 12th International Fluid Power Conference, Dresden, Germany, 12–14 October 2020; Volume 2. [CrossRef]
28. Virtanen, P.; Gommers, R.; Oliphant, T.E.; Haberland, M.; Reddy, T.; Cournapeau, D.; Burovski, E.; Peterson, P.; Weckesser, W.; Bright, J.; et al. SciPy 1.0: Fundamental algorithms for scientific computing in Python. *Nat. Methods* **2020**, *17*, 261–272. [CrossRef] [PubMed]
29. Johnston, N. The Transmission Line Method for Modelling Laminar Flow of Liquid in Pipelines. *Proc. Inst. Mech. Eng. Part I J. Syst. Control. Eng.* **2012**, *226*, 586–597. [CrossRef]